Les Cahiers du GERAD ISSN: 0711–2440

Simulation of weathered profiles coupled with multivariate block-support simulation of the Puma Nickel Laterite Deposit, Brazil

M. de Freitas Silva
R. Dimitrakopoulos

G–2015–90

September 2015

GERAD HEC Montréal
3000, chemin de la Côte-Sainte-Catherine
Montréal (Québec) Canada H3T 2A7

Tél. : 514 340-6053
Téléc. : 514 340-5665
info@gerad.ca
www.gerad.ca

Simulation of weathered profiles coupled with multivariate block-support simulation of the Puma Nickel Laterite Deposit, Brazil

Mario de Freitas Silva [a,c]
Roussos Dimitrakopoulos [a,b]

[a] *COSMO – Stochastic Mine Planning Laboratory, Department of Mining and Materials Engineering, McGill University, Montreal (Quebec) Canada, H3A 2A7*

[b] *and GERAD*

[c] *Now with Vale SA, Belo Horizonte, Brazil*

roussos.dimitrakopoulos@mcgill.ca

September 2015

Les Cahiers du GERAD
G–2015–90

Abstract: Modeling and assessing spatial uncertainty of mineral deposits is critical for capital investments in mining projects. However, traditional approaches for modeling geological domains and geostatistical estimation provide smoothed representations of the deposit and ignore spatial variability, hence mislead downstream decisions. Spatial variability and related uncertainty in modelling mineral deposits can be quantitatively described by stochastic spatial simulations. This is demonstrated through an application to the Puma deposit, a major nickel lateritic asset in Brazil. To integrate the variability of the regolith profiles of the deposit, their thicknesses are calculated after an unwrinkling process is applied and the deposit is then jointly simulated using min/max autocorrelation factors (MAF). The realizations serve as geological boundaries within which Ni, Co, Fe, SiO_2, MgO and Dry-tonnage factor (DTF) are subsequently jointly simulated directly at block support scales. The final result is a series of equiprobable representations of the deposit that incorporate both grade and tonnage uncertainty. These simulations can be used to assess the uncertainty about key aspects of the project, such as the strict control of the ore's quality that feeds the ferronickel processing plant. The framework explored herein takes advantage of the MAF and direct block simulation approaches which facilitate the joint simulation of large multivariate deposits for industrial environments.

Key Words: Nickel laterite, joint simulation, min/max autocorrelation factor, direct block simulation, unwrinkle.

1 Introduction

Over the years, stochastic simulation has been shown to be an important tool for assessment of spatial geological uncertainty in mineral deposits. Modelling uncertainty leads to a better understanding and quantification of risks at different decision levels in mining, such as in grade-tonnage curves, mine planning, grade control, etc. (e.g., Journel, 2007; Peattie and Dimitrakopoulos, 2013)

In several cases, it is of interest to model the spatial variability of not only one but a set of multiple spatially correlated variables. In contrast to the univariate case, traditional methods for multivariate simulation show cumbersome features that limit their practical use in the industrial environment (Boucher and Dimitrakopoulos, 2012). The main contributors for this complexity are the impractical computational requirements and tedious inference of an explicit model of corregionalization, which substantially increases with the number of attributes being jointly simulated (Goovaerts, 1997).

An alternative to those co-simulation frameworks is to transform the initial set of spatially correlated attributes into a new set of uncorrelated (orthogonal) factors. These factors are independently modelled and simulated, and later back-transformed to the original space of the multivariate dataset, aiming the reproduction of their cross correlations. Earlier efforts in multivariate geostatistics using such strategy are based on Principal Component Analysis (PCA) (David, 1984, 1988). Although this methodology is simple to implement, it can only guarantee that the factors are uncorrelated at lag zero but not for all separation distances, except under very specific cases such as when assuming an intrinsic model of corregionalization (Goovaerts, 1993; Wackernagel, 2003). Leuangthong and Deutsch (2002) use a stepwise conditional transformation (SCT) to transform the data into multiGaussian variables uncorrelated at lag zero. Among the main drawbacks associated to this step-wise transformation are: the need of a large amount of data required when dealing with several variables and the fact that, as other global transformation procedures, it may deteriorate some existing local spatial connectivity of the grades. With similar goals as SCT but solving the curse of dimensionality, Barnett and Deutsch (2014) use a projection pursuit algorithm (PPMT) to iteratively search for 'least gaussian' structures of the multivariate distribution and sequentially "gaussianize" them. Such a process eventually transforms the multivariate data into a multivariate Gaussian distribution decorrelated at lag zero, but nevertheless that still carries a spatial structure. Tercan and Sohrabian (2013) use Independent Component Analysis (ICA) to find *non-gaussian* factors that are mutually independent (hence uncorrelated) at lag zero. In a different way than in previous frameworks (SCT and PPMT) that rely on a multiGaussian based algorithm to independently simulate the factors, here the authors use a direct simulation algorithm.

Aiming to find factors that are uncorrelated not only for lag zero but also at any other distance, Desbarats and Dimitrakopoulos (2000) utilize minimum/maximum autocorrelation factors (Switzer and Green, 1984) in a geostatistical context. Relying on the linear model of corregionalization (LMC) for the multivariate random field, MAF is able to provide a set of factors uncorrelated at any distance. Stochastic simulations through MAF has been increasingly used in a series of other geostatistical studies, mostly using a Multi-Gaussian framework for the independent simulation of the uncorrelated factors (Dimitrakopoulos and Fonseca, 2003; Eggins, 2006; Lopes et al., 2011; Goodfellow et al., 2012). Observing the fact that the orthogonalization does not relies on multinormality of the random field, in Bandarian et al. (2008) MAF transformation is directly applied to the dataset, without prior transformation to Gaussian space, and proceeding with a direct simulation algorithm afterwards. Although the approach reduces reliance on the multiGaussian paradigm, it suffers with the pitfalls related to direct simulation techniques. Rondon (2012) provides a thorough review about the MAF transformation. An alternative methodology is suggested by Mueller and Ferreira (2011), who explore the application of an approximate joint diagonalization technique (AJD) called U-WEDGE. This method sets out to find a rotation matrix which is able to simultaneously diagonalize (approximately) a set of symmetric matrices corresponding to the series of cross-semivariograms at different lags.

For mineral deposits, the target support to be simulated (selective mining unit) is usually much larger than the available drilling data (typically considered as point support). Thus, the common practice consists on simulating the entire deposit at point supports followed by a post-processing step to average them out inside each of the mining blocks. Such approach can be cumbersome in practical terms when large deposits are simulated, comprising several millions of blocks. A simulation alternative for univariate multiGaussian

random fields directly at block support is proposed in Godoy (2002) and extended to the joint simulation with MAF in Boucher and Dimitrakopoulos (2009, 2012), significantly increasing efficiency and reducing memory requirements during the simulation.

This paper details the application of MAF and direct block simulation for modelling the joint spatial uncertainty of multiple geological attributes of Puma, a major nickel laterite deposit in Brazil. The nickel enrichment is result of intensive weathering and laterization of ultramafic ridge complexes within the Amazon Craton of the Brazilian Precambrian Shield. Above the bed rock, a saprolitic zone is found, characterized by high content of Nickel, relatively high silica and magnesia and low iron contents. Near to the surface, an iron-rich unit is formed, with a lower nickel, silica and magnesia contents. The supergene enrichment of the regolith, leaching and erosional processes result in a highly complex environment, which accounts with a large spatial variability of thicknesses and grades.

Due to the great disparity of their chemical composition, very different metallurgical routes are needed to process limonitic or saprolitic ore. In its current operation, the mine produces ferronickel from the saprolitic ore, while the limonitic ore type is treated as an opportunity material. The process efficiency is extremely sensitive to the head grades, requiring a strict control over the quality of the ore feed, which reinforces the necessity of jointly modelling the spatial variability of multiple elements.

The following sections include a summary of the joint simulation framework through MAF and its extension for direct block simulation; a thorough description of the deposit and available data; joint simulation of bottom layers of limonite and saprolite domains, by means of modelling their respective thicknesses, followed by subsequent joint simulation of Ni, Co, Fe, SiO_2, MgO and Dry-Tonnage Factor (DTF), aiming to a geological plausibility of the complex orebody and control over operational quality required by the ferronickel plant. Thereafter, the results from the generated grade-tonnage curves are discussed, followed by conclusions.

2 A recall on joint simulation of multiple correlated attributes through min/max autocorrelation factors (MAF)

Let $Z(u) = [Z_1(u), Z_2(u), \ldots, Z_K(u)]^T$ denote a stationary and ergodic random field (RF) over a region D, representing K correlated continuous attributes of a natural phenomenon measured on isotopic point support samples. Now, consider its pointwise normal score transformation $Y(u) = [Y_1(u), \ldots, Y_K(u)]^T = [f_1(Z_1(u)), \ldots, f_K(Z_K(u))]^T$, which is deemed a multiGaussian RF with zero mean and unit variance. The minimum/maximum autocorrelation factors $M_{MAF}(u)$ are defined as pairwise orthogonal linear combinations of the Gaussian variable $Y(u)$ as following (Desbarts and Dimitrakopoulos, 2000):

$$M_{MAF}(u) = A^T Y(u). \tag{1}$$

For which the coefficients of the transformation matrix A are obtained from:

$$A^T = Q_2^T \wedge_1^{-1/2} Q_1^T \tag{2}$$

where Q_1 and $\wedge_1$ are respectively the matrices of eigenvectors and eigenvalues obtained from the spectral decomposition of the symmetric covariance-variance matrix B of the RF $Y(u)$ at zero lag distance. Matrix Q_2 is the matrix of eigenvectors resulted from the following spectral decomposition:

$$\wedge_2 = Q_2 \Gamma_{P_{PCA}}(\triangle) Q_2^T \tag{3}$$

where matrix $\Gamma_{P_{PCA}}(\triangle)$ is an experimental variogram matrix at lag $\triangle$ for PCA factors derived from:

$$P_{PCA}(u) = \wedge_1^{-1/2} Q_1^T Y(u). \tag{4}$$

In practice, to ensure that the transformed variables are orthogonal at all distances, several experimental lags $\triangle$ must be tested, selecting the one which provides the best decorrelation of the factors. This 'data-driven' approach of MAF avoids the tedious modelling and fitting of a linear model of corregionalization, since the transformation matrix is directly derived from the experimental data.

These new defined factors $M_{MAF}(u)$ can be independently modelled and simulated since they are spatially uncorrelated for any distance. Moreover, because of the initial multiGaussian assumption, they also follow the same distribution law, which allows the use of sequential Gaussian simulation (SGS) to provide point support realizations for each factor. More general and efficient frameworks can also be applied such as direct block simulation.

2.1 Direct block simulation

Aiming to increase efficiency and to alleviate computational requirements associated to memory and data management during geostatistical simulation, Godoy (2002) has proposed a direct block simulation framework (DBSim). This method produces univariate simulations of multiGaussian random fields. Boucher and Dimitrakopoulos (2009) have extended the idea for direct block simulation of multiple correlated variables, independently simulating the MAF factors for each of the blocks inside the domain. Thus, the simulation at block-support scale using MAF calls for the block support RF $Z_V(v)$ defined as following:

$$Z_V(v) = \frac{1}{N}\sum_{i=1}^{N} \phi^{-1}\left[\left(A^T\right)^{-1} M_{MAF}(u_i)\right], \qquad u_i \in v, \forall i \tag{5}$$

where each block $V \in D$ is discretized by a set of N points indexed by u_i.

The algorithm follows a random path to visit each of the blocks inside the domain and, for each one of the factors (indexed by $l = 1 \dots k$), the N discretizing points are simulated by performing a joint LU simulation (Myers, 1989). Intuitively, it can be seen as a pointwise simulation using an extension of the generalized group sequential Gaussian simulation (Dimitrakopoulos and Luo, 2004), implementing joint LU to incorporate conditioning information at different supports (samples and internal nodes at point support plus previously simulated blocks). Let C^l_{IIVV} be the covariance matrix of all conditioning information and C^l_{pIV} the covariance matrix between the discretizing nodes and the neighboring information at point and block supports for the l^{th} factor. Those can be expanded as:

$$C^l_{IIVV} = \begin{bmatrix} {C_{II}}^l & {C_{IV}}^l \\ {C_{VI}}^l & {C_{VV}}^l \end{bmatrix} \text{ and } C^l_{pIV} = \begin{bmatrix} {C_{pI}}^l & {C_{pV}}^l \end{bmatrix} \tag{6}$$

where ${C_{II}}^l$, ${C_{IV}}^l$ and ${C_{VV}}^l$ are point-to-point covariance matrices, point-to-block, and block-to-block covariances, respectively for the l^{th} factor; ${C_{pI}}^l$ and ${C_{pV}}^l$ are the covariances between the discretizing nodes and the neighboring information at point and block supports respectively.

Finally, the vector of N simulated factors ${m_p}^{l*}$ inside a given block for each factor l, is obtained by solving the following system of equations (Godoy, 2002; Boucher and Dimitrakopoulos, 2009):

$${m_p}^{l*} = {L_{21}}^l \left({L_{11}}^l\right)^{-1} {m_{IV}}^l + {L_{22}}^l w \tag{7}$$

where ${m_{IV}}^l$ is the vector containing neighboring samples at point support and previously simulated blocks for the factor l, w is a vector of random numbers following a standard normal distribution and ${L_{21}}^l$, ${L_{11}}^l$ and L_{22} are obtained from the following Cholesky decomposition:

$$\begin{bmatrix} {C_{IIVV}}^l & {C_{IVp}}^l \\ {C_{pIV}}^l & {C_{PP}}^l \end{bmatrix} = \begin{bmatrix} {L_{11}}^l & 0 \\ {L_{21}}^l & {L_{22}}^l \end{bmatrix} \begin{bmatrix} {L_{11}}^{lT} & {L_{21}}^{lT} \\ 0 & {L_{22}}^{lT} \end{bmatrix} \tag{8}$$

One may note that, once the conditioning neighbourhood is retrieved, the system of equations shown in (7) and (8) must be solved k times, one for each factor l. Moreover, it is important to note that, because the simulation process is conditioned by previously simulated blocks at MAF space and that, there is no direct transformation from this orthogonal space to the original space of the multivariate attributes at block support, after the simulation of internal nodes, the process must be split in two parts: (1) the block values $M^{l*}_V(v)$ for each one of the factors are obtained by averaging the simulated factors ${m_p}^{l*}$ at point supports,

and (2) the internal nodes are back rotated to the data space and averaged to generate the desired block values as previously shown in equation (5).

The direct block MAF simulation algorithm proceeds as following:

1. Transform the data $Z(u)$ to normal scores $Y(u)$.
2. Orthogonalize $Y(u)$ through MAF transformation to obtain $M_{MAF}(u)$.
3. Define a random path visiting each block.
4. For each block V, simulate for each factor l the discretizing N internal points ${m_p}^{l*}(u_i)$, $i = 1, \ldots, N$, using the LU decomposition as shown in (8). Afterwards:
   (a) For each factor l, average ${m_p}^{l*}(u_i)$ over the block to obtain the simulated block values $M_V^{l*}(v)$ for each corresponding factor.
   (b) Back-transform of ${m_p}^{l*}(u_i)$ at all discretizing nodes and for all factors, in order to obtain the simulated block value $Z_V^*(v)$ as in equation (5).
5. Repeat step 4 until all blocks are simulated.

3 Simulation of the Puma Nickel Laterite Deposit

3.1 Deposit description and data available

The lateritic deposit studied herein (Puma) is located in northern Brazil and it has developed from layered ultramafic complexes intruding Pre-Cambrian Brazilian shield. Supergene and residual concentrations of nickel have developed along an elongated ridge for some 23 km, for which only 3.5 km are comprised in this study. The ridge is an elevated area with its northerly slopes range up to 30°–45° and its southerly slopes 10°–15°. An important characteristic of the deposit are extensive silica caps on the ridges, which was likely responsible to preserve saprolitic ores from erosion (Canico Resources Corporation [CRC], 2005). The main structures of variability of the deposit are controlled by the geometry of the ridge, which was aligned along East-West. The vertical direction comprises the direction of major variability.

The data set used in this study comprises 1 938 drill holes with 59 821 core samples regularized in interval lengths of 1 m, assayed for Ni, Co, Fe, SiO_2, MgO and Dry-Tonnage-Factor (DTF). For confidentiality reasons the grades and DTF were modified by a constant factor. The vertical drill holes retrieved for this study cover an area of approximately 4.8 km^2 (Figure 1). The holes are at shallow depths (mode of approximately 9.0 m) and the sampling grid spacing is approximately 25 m in most of the areas of the ridge. In some denser areas, the separation can be as close as 6 m and approximately 100 m in more external parts of the deposit.

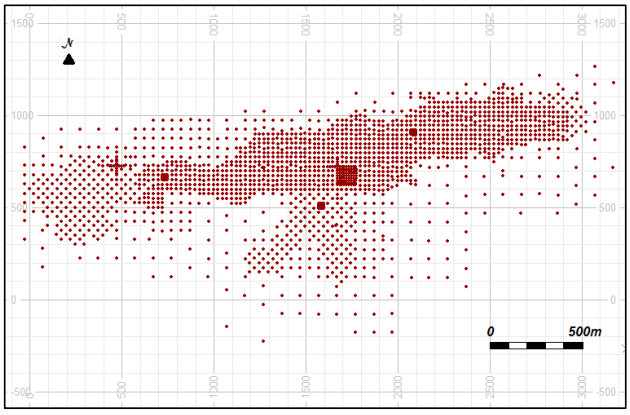

Figure 1: Plan view showing the drill hole locations along the deposit ridge.

The lithologies are grouped according to their characteristics and they can be simplified into three distinct layers:

a. Limonite (Rock Code = 0), which is the uppermost horizon and has been completely altered by chemical weathering. Primary textures are absent, with iron-rich minerals increasing to the top, becoming pisolitic. It contains some nickel, low MgO and high Fe.
b. Saprolite (Rock Code = 1), which is the primary source of nickel for the ferronickel process in the actual mine. Zone with somewhat altered bed rock, with preserved structures and textures of minerals. It is rich in hydrous Mg silicates. Shows a low content of Fe and high MgO.
c. Bedrock (Rock Code = 2), which is the parental rock lightly weathered. It can be characterized by low nickel grades, high MgO and low Fe.

3.2 Joint simulation of weathered profiles

In this section, the main goal is to simulate the geometry of the main lateritic units in order to model their joint spatial uncertainty. This is accomplished by jointly simulating the bottom surfaces of limonite and saprolite. It is noteworthy that the weathering and leaching mechanisms in lateritic deposits, usually act in a way that bottom layers of the lateritic domains are well correlated to the topography. This reference level can be treated as a regional trend, thus, the bottom layers are modelled in terms of its residual part, which corresponds to the thickness. In other words, the thicknesses of the different profiles of the regolith are stochastically modelled and subtracted from the topography in the end.

In addition, one may recall that the vertical drillholes do not directly capture the true thicknesses of the geological units, hence, the sample thicknesses are calculated after applying an *unwrinkle* process to the bottom levels using the topography level as reference (Deutsch, 2005). After simulating, the thicknesses are added back to the "flattened" topography in order to generate the bottom layers' elevations of each unit. Then, those layers are "folded" back to the original space of the deposit, and they are taken as reference levels to build the categorical orebody models at block support of $12 \times 12 \times 3$ m^3.

In order to extract representative univariate statistics of the thickness for both limonite and saprolite units, declustering cells of 25 m are used. Table 1 brings a summary of these declustered statistics. As one may note, both distributions are positively skewed, with limonite showing a higher variability. One important feature from the distributions is the remarkable discontinuity at the origin. This is shown in Table 1 as the percentage of missing thicknesses, which relates to the percentage of locations where each profile is absent. These "missing thicknesses" are mostly associated with eroded locations, mainly located at steep slopes. As mentioned above, besides the fact that it is the uppermost geological unit, the limonite is also more easily eroded than the saprolite, because the latter is protected by a siliceous cap over it.

Table 1: Summary of declustered statistics for True Thickness (TTK) of main units .

	Mean (m)	**CV**	**Skewness**	**Kurtosis**	**Min (m)**	**P 25 (m)**	**P 50 (m)**	**P 75 (m)**	**Max (m)**	**Missing TTK (%)**
Limonite	2.41	1.23	2.73	12.15	0	0	1.98	3.02	28	35.55
Saprolite	9.22	0.72	1.27	2.04	0	4.52	7.67	12.52	45	2.44

The global correlation between the thicknesses of both units is practically absent ($\rho < 0.1$). At first glance, as the thicknesses showed no correlation, they could be simulated independently on the basis of their individual regionalization, but nevertheless this could lead to some geological inconsistencies where local correlations exist. For example, information such as absence of limonite actually increases the probability of also eroded saprolite. In this study, it has been decided to jointly simulate saprolite and total thicknesses, with the limonite being indirectly obtained by subtracting the saprolite from the total thickness. Figure 2 brings a scatterplot showing the correlation between those variables:

3.2.1 Normal score and MAF transformations of thicknesses

Prior to applying MAF transformations to the spatially correlated variables, each of them are transformed to a standard normal distribution. It is noteworthy that, the correlation between the normal score variables are

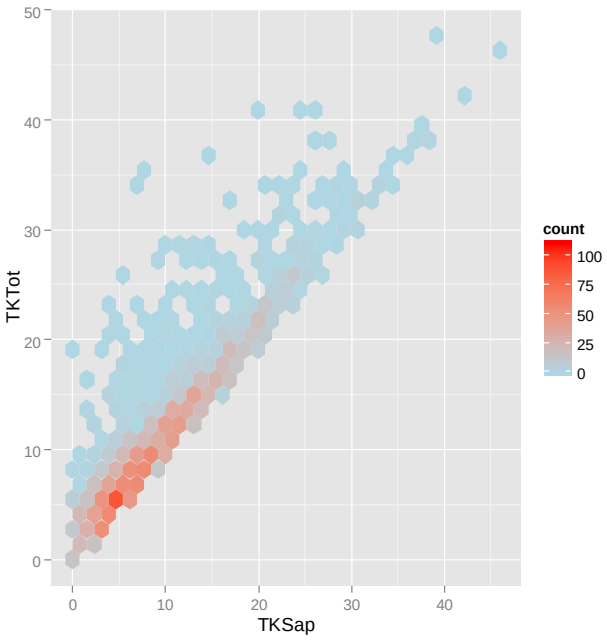

Figure 2: Scatterplot for Saprolite and Total thicknesses ($\rho = 0.92$).

kept very similar to the ones in the data space ($\rho = 0.90$), which suggests that the correlation is well preserved after the transformation. The lag distance ($\triangle$) used in Eq. (3) is 25 m and is derived after experimentally testing several distances to assure suitable decorrelation of the MAF factors. The omnidirectional correlogram between them is depicted in Figure 3, showing the absence of correlation over all distances.

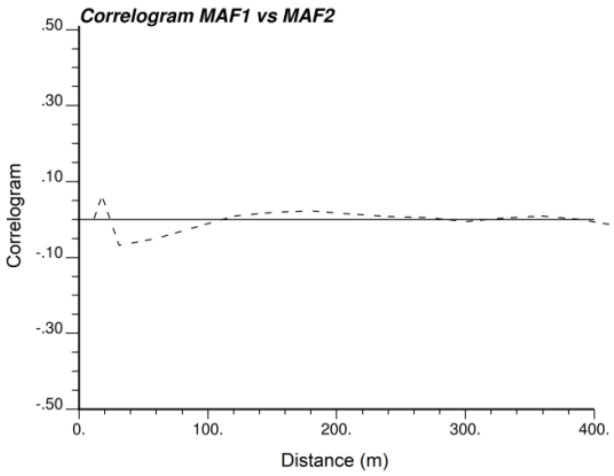

Figure 3: Correlogram between MAF1 and MAF2.

Figure 4 shows the experimental variograms of each factor fitted by their respective models. They both are assumed to contain a nugget and a spherical structure. One may note that MAF1, which has the larger eigenvalue associated to it, absorbs great part of the variance, which is revealed by its smaller spatial continuity if compared to MAF2.

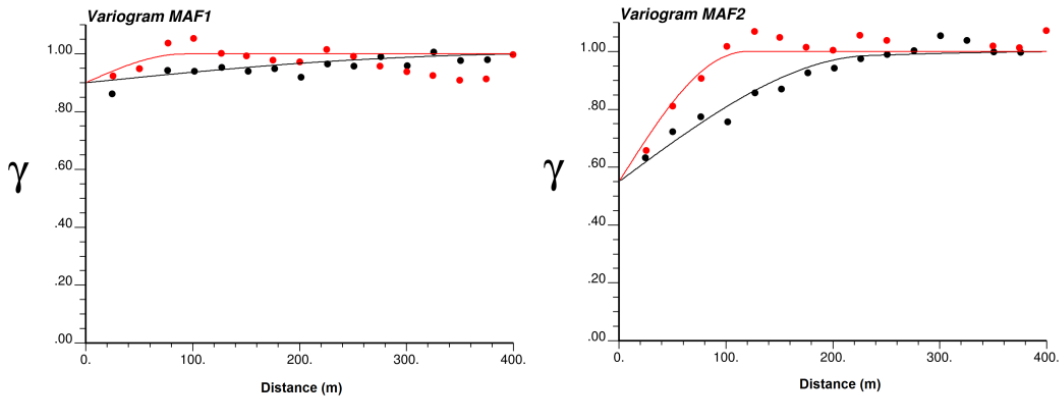

Figure 4: Experimental variogram (dotted) and fitted models (lines) of each MAF factor for the main directions, NS (gray) and EW (black).

3.2.2 Conditional simulation of MAF factors

Conditional simulation is independently performed on the two MAF factors using the pointwise sequential gaussian simulation (SGS) on a grid of 3×3 m^2, resulting in a total of approximately 400,000 nodes. Five simulations are generated for each factor. The validation of MAF simulations is not presented herein since the subsequent sections show the validation of realizations directly in data space.

3.2.3 Validation of simulated thicknesses

In addition to a visual inspection, validation of jointly simulated variables involves the calculation of univariate distributions, experimental variograms and cross-variograms of the simulated realization in the data space to ensure the reproduction of statistics inferred from the original data. Figure 5 shows that both declustered cumulative distributions of saprolite and total thicknesses are well reproduced by the simulated models.

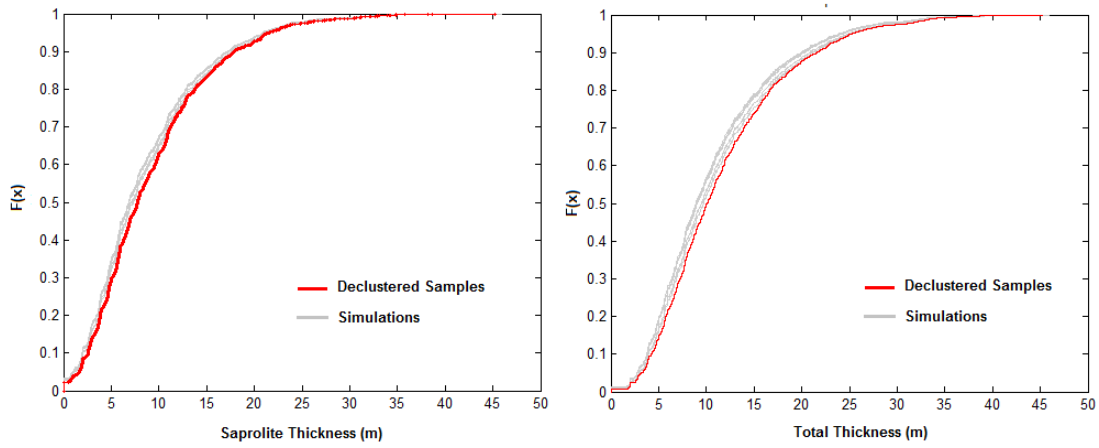

Figure 5: Cumulative distributions of declustered data in red and simulated models in gray for saprolite (left) and total thickness (right).

Figures 6 to 8 show that the conditional simulations honour the variograms and cross-variograms of the original drillhole data. Recall that the variograms and cross variograms of the original variables are not directly used during the simulation, since it only requires the variograms of the uncorrelated MAF factors.

In a post-processing step, the limonite thicknesses are derived from the subtraction of the saprolite from the total thickness. The validation of its spatial variability and univariate distribution are depicted

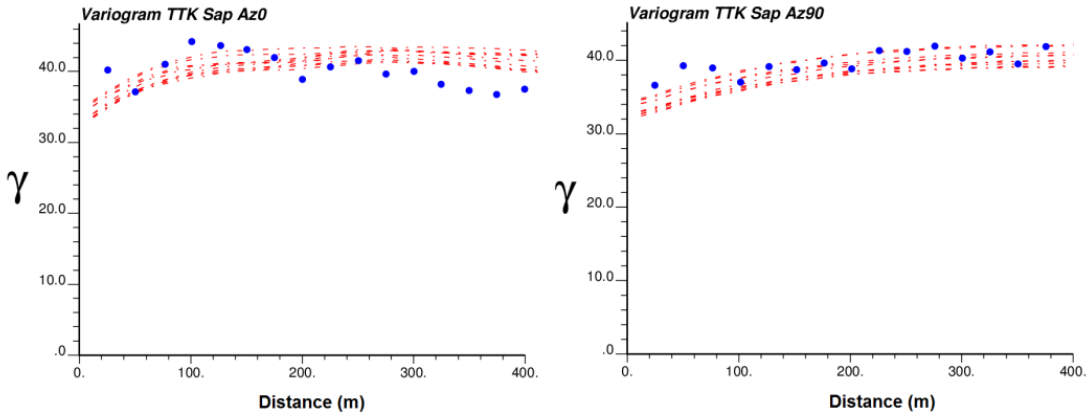

Figure 6: Experimental variogram (black dots) and simulated models (gray dashed lines) for Saprolite thickness along the main directions NS and EW.

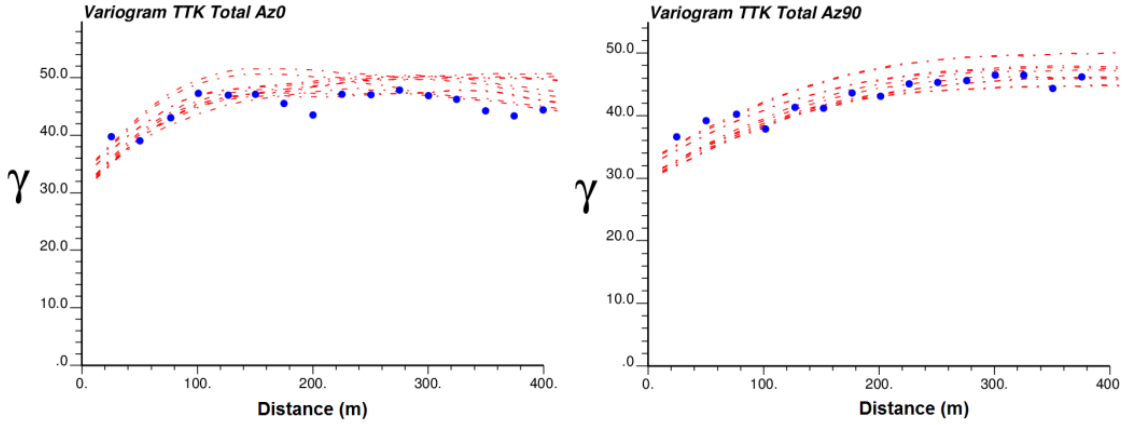

Figure 7: Experimental variogram (black dots) and simulated models (gray dashed lines) for Total thickness along the main directions NS and EW.

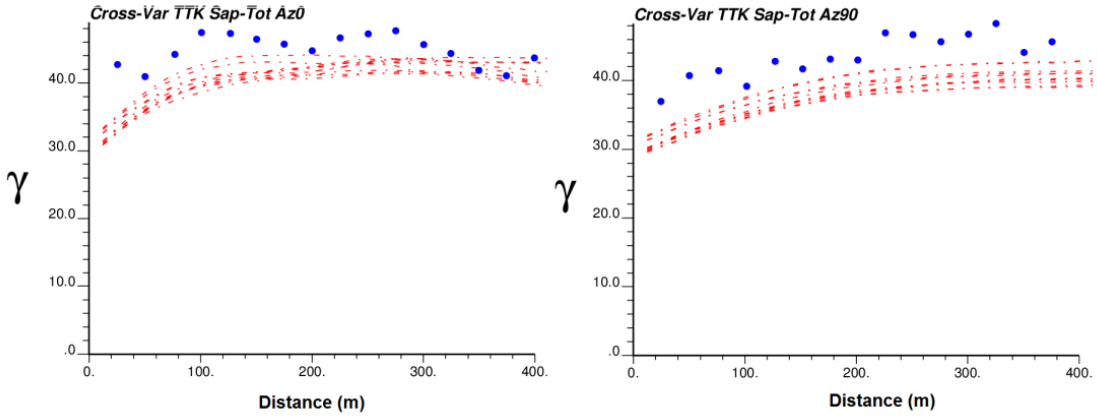

Figure 8: Experimental cross-variograms (black dots) and simulated models (gray dashed lines) between Saprolite and Total thicknesses along the main directions NS and EW.

in Appendix A. In addition to this, the indicator variograms of the categorical model generated after back transforming the simulated bottom layers of the mineralized units, are also well reproduced.

3.3 Multivariate block-support simulation of grades and Dry-Tonnage factor

Joint simulations directly on the block support ($12 \times 12 \times 3$ m^3) for Ni, Co, Fe, MgO, SiO_2 and Dry-Tonnage-Factor, are constrained by previously simulated saprolite and limonite units. Although the actual mine operates a pyrometallurgical plant and only saprolitic ore is processed, the joint simulation of the elements inside the limonitic horizon is motivated by the fact that it is actually enriched in nickel and that such approach may lead to a better model of dilution. As mentioned previously, a strict control of the silica (SiO_2) to magnesia (MgO) ratio and iron (Fe) content is required to ensure minimal disruptions of the ferronickel plant.

Figure 9 shows the declustered distribution of the main attributes of interest for the processing plant (Nickel, Iron, SiO_2:MgO ratio), inside the different lithological units.

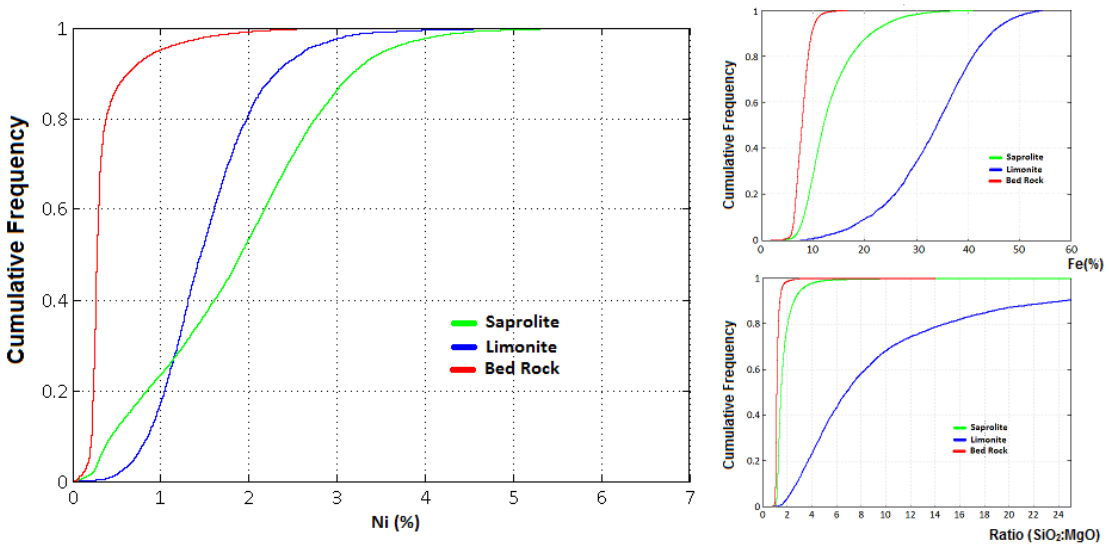

Figure 9: Distribution of the samples' Ni grades over the different lithological horizons.

These curves highlight the dissimilarities of the populations inside the different weathered profiles of the Ni laterite. It clearly shows that limonite and saprolite are the main horizons enriched in Nickel. Saprolite shows a higher Ni average grade and variability than the limonite. The opposite behavior is verified for the iron content and Si:Mg ratio.

Vertical trends are commonly seen in laterite nickel studies. For this case study in particular, trends inside the saprolitic unit are not as significant as the ones found for the limonite. Therefore, inside this latter unit, the simulation is carried out on the residuals of each attribute after modeling their respective trends. The scatterplot matrix showing their multivariate correlation between the elements inside each domain are depicted in Figure 10, also highlighting both Pearson and Spearman (ranked) correlation coefficients.

As expected, Figure 10 shows that the correlations between the elements may significantly vary from one geological unit to the other. For instance, even though nickel shows a moderate correlation to most of the other elements inside the saprolite horizon, it shows very low correlations with Co and Fe for the limonite.

3.3.1 Normal score and MAF transformations of multi-elements

Similar to the steps carried out for the simulation of thicknesses, each of the attributes modeled herein is transformed to normal score space. Recall that for the limonite, the variables considered are the residuals obtained for each element after subtracting their modelled trends.

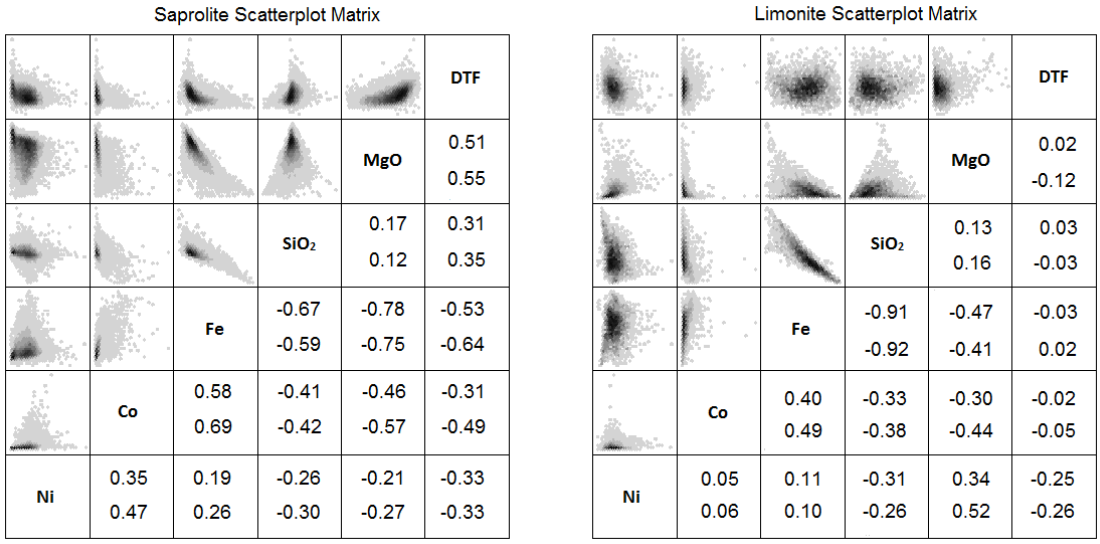

Figure 10: Scatterplots of elements modeled (upper diagonal pannel) and correlation coefficients in lower diagonal pannel, with Pearson above and Spearman below, for both geolocial units, Saprolite and Limonite.

For deriving the loading matrix of the MAF transformations, a lag distance ($\triangle$) of 25 m is used in Eq. (3), the same values as in the joint simulation of thicknesses. Figure 11 shows that, there are no spatial cross-correlations between the six different factors inside each geological unit, suggesting that the MAF factors have been successfully decorrelated.

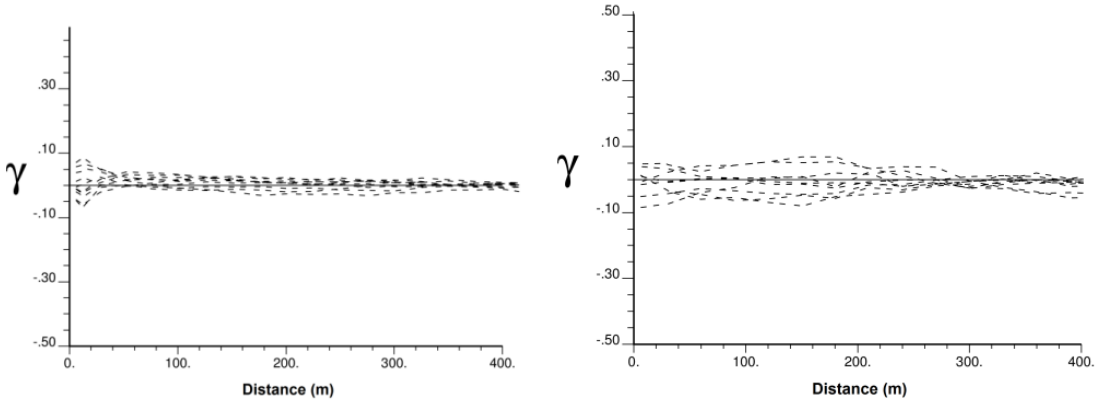

Figure 11: Omnidirectional correlogram between MAF factors taken in pairs for saprolite (left) and limonite (right).

The variography on each factor are performed and the experimental variograms are fitted using exponential models. Those variograms are shown in Appendix B.

3.3.2 Conditional simulation of MAF factors

Conditional simulations for each of the factors in each of the domains previoulsy simulated are performed independently using Eq. 7 and averaged into blocks using Eq. 5. Five simulations are generated inside each geological unit (total of $5 \times 5 = 25$ simulations) using blocks of $12 \times 12 \times 3$ m^3 and a $4 \times 4 \times 3$ node discretization, resulting in an an average of 50 and 20 thousand blocks inside saprolite and limonite units,

respectively. For comparison, at point support scale, this corresponds to a simulation of about 900,000 and 2,500,000 nodes inside each of these geological units.

It is noteworthy that, for the case of limonite, an additional step is needed during the direct simulation at block support. In Eq. 5, besides the back transformations from MAF and normal score spaces, the trend also need to be added back to the simulated residuals at the discretizing nodes, before their average is calculated to obtain the simulated block value in data space. Once again, the validation of MAF simulations is not presented herein since the subsequent sections show the validation of realizations directly in data space.

3.3.3 Validation of multi-elements simulation

For validations purposes, the point-scale simulated values for some simulations in both saprolite and limonite units are retrieved. Then, the same validations performed for the simulation of thicknesses in Section 3.2 are repeated herein in the data space. Figure 12 shows that the cumulative distributions of each simulated attribute honour the declustered statistics infered from the drillholes with some ergodic fluctuations.

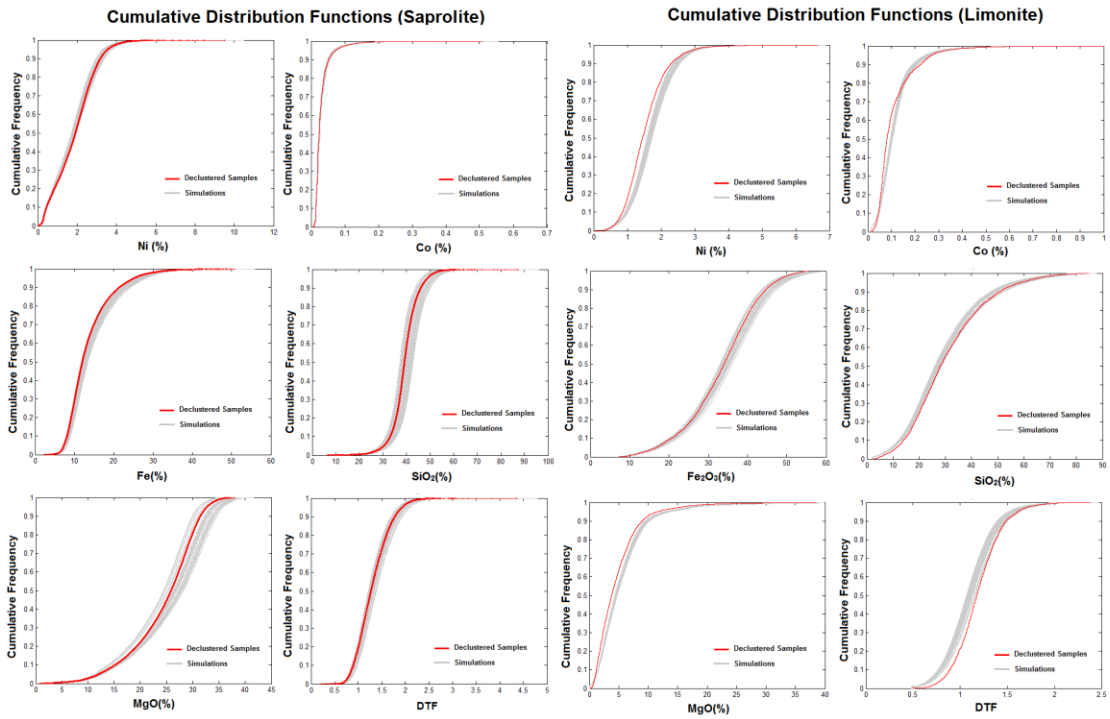

Figure 12: Experimental cumulative distribution functions of declustered samples (black) and simulated models at point supports (gray) for saprolite (left) and limonite (right).

Figures 13 to 16 show some plots of variograms and cross-variograms for drillhole samples and conditional simulations at point support scales inside the saprolite unit. All results suggest that geostatistical realizations are able to reproduce the main spatial features seen for the original data.

The reproduction of spatial statistics for the limonite are also very good, but for the sake of brevity, only the vertical variogram of nickel and its cross variogram with MgO are shown in Figure 17, in order to highlight the reproduction of remarkable 'drifts' seen in these experimental variograms of the data.

3.4 Visualization of conditional simulations

Figure 18 shows the example of a joint simulation at block support scale for the different lateritic zones and a joint simulation of Ni, Fe and SiO_2:MgO constrained by it. As suggested by the data set, the plan view of categorical simulation shows how saproltite tends to outcrop at the surface in many places where

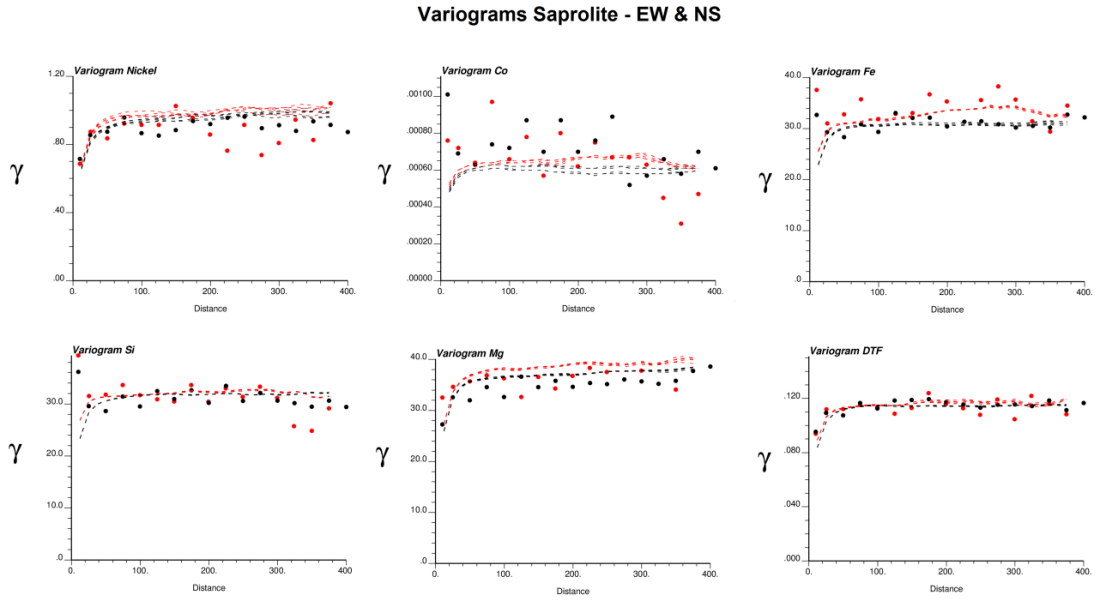

Figure 13: Saprolite – Experimental direct variograms (dotted) and point-support simulated models (lines) for each element in data space over the horizontal direction (NS in gray and EW in black).

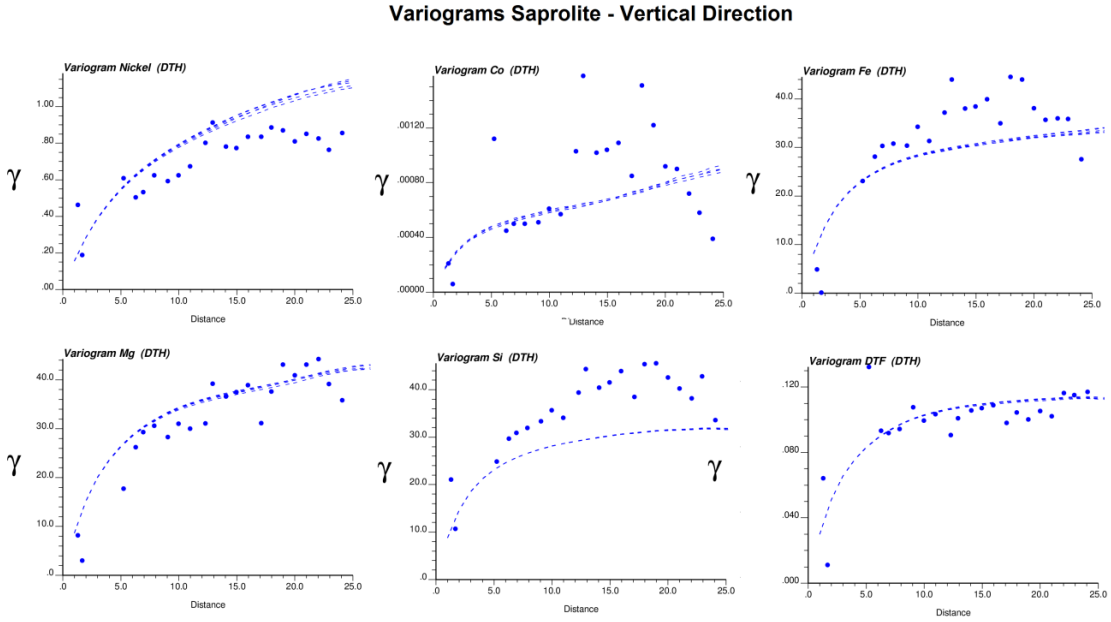

Figure 14: Saprolite – Experimental direct variograms (dotted) and (point-support) simulated models (lines) for each element in data space along the vertical direction.

limonite was eroded because of the steep relief . The other plan views for the continuous elements split the simulations inside each of the lateritic zones. Thus, the most of the saprolite shown in those maps actually lies underneath the limonite layer. These maps highlight the spatial differences between limonite and saprolite and reinforce the previous validations, which suggests that the simulated models honour the spatial features from the dataset.

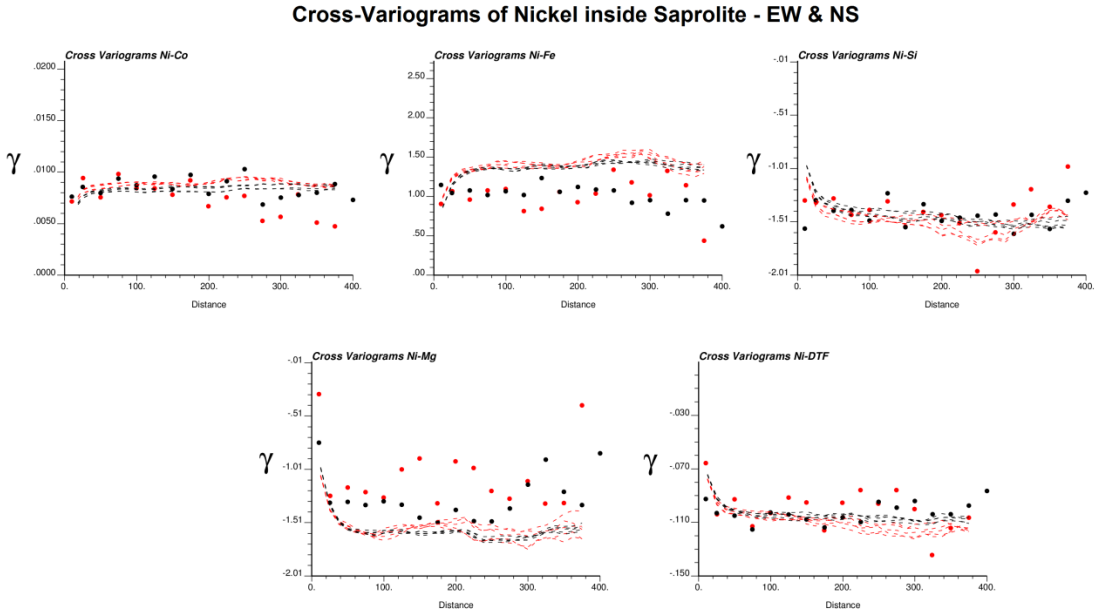

Figure 15: Saprolite – Experimental cross-variograms (dotted) and point-support simulated models (dashed lines) for nickel and other five elements, in data space, over the horizontal direction (NS in gray and EW in black).

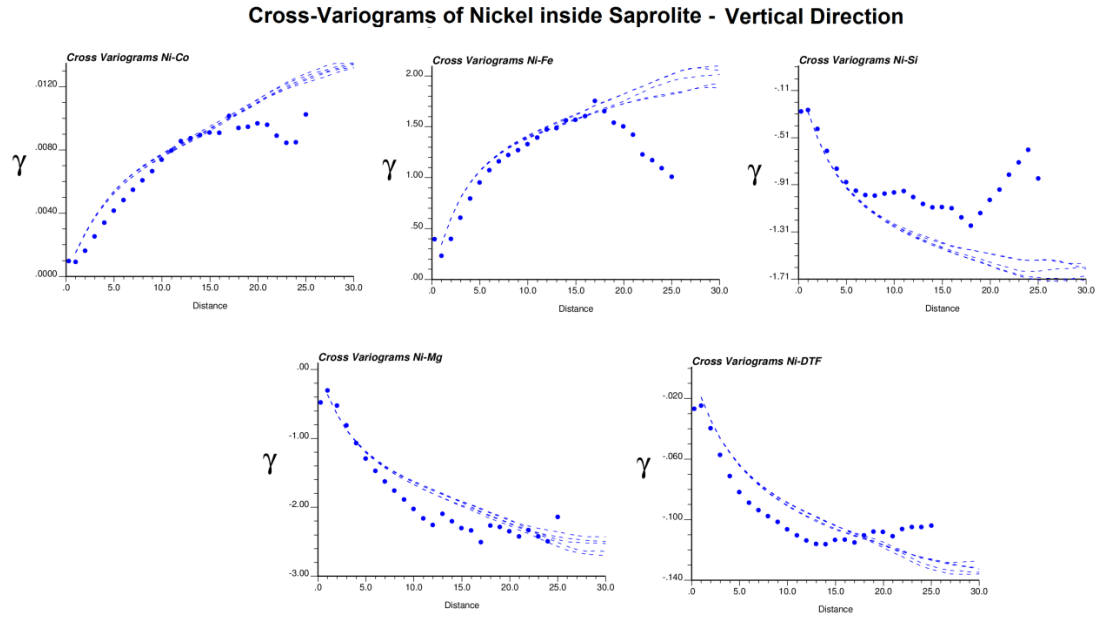

Figure 16: Saprolite – Experimental cross-variograms (dotted) and point-support simulated models (dashed lines) for nickel and other five elements, in data space, along the vertical direction.

3.5 Risk assessment results and discussion

In lateritic nickel deposits, a strict control of SiO_2, MgO and Fe grades is required. The range of grades for those key elements may vary accordingly to the metallurgical route designed for the project. The entire mining project that includes the deposit considered in this study (Ona-Puma complex), represented a total investment of about $2.3 billion dollars. The operation produces ferronickel via rotary kiln-electric furnace

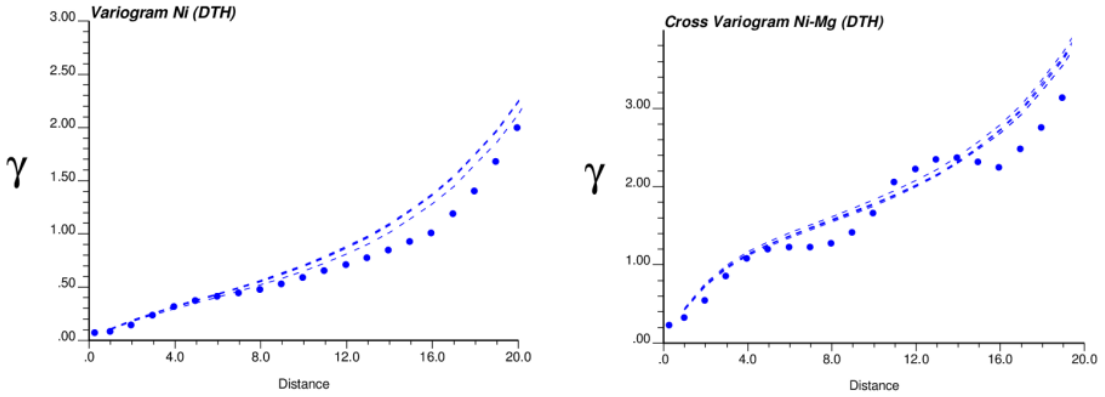

Figure 17: Limonite – Experimental Ni variograms and Ni-Mg cross-variograms (dotted) and point-support simulated models (dashed lines), in data space, along the vertical direction.

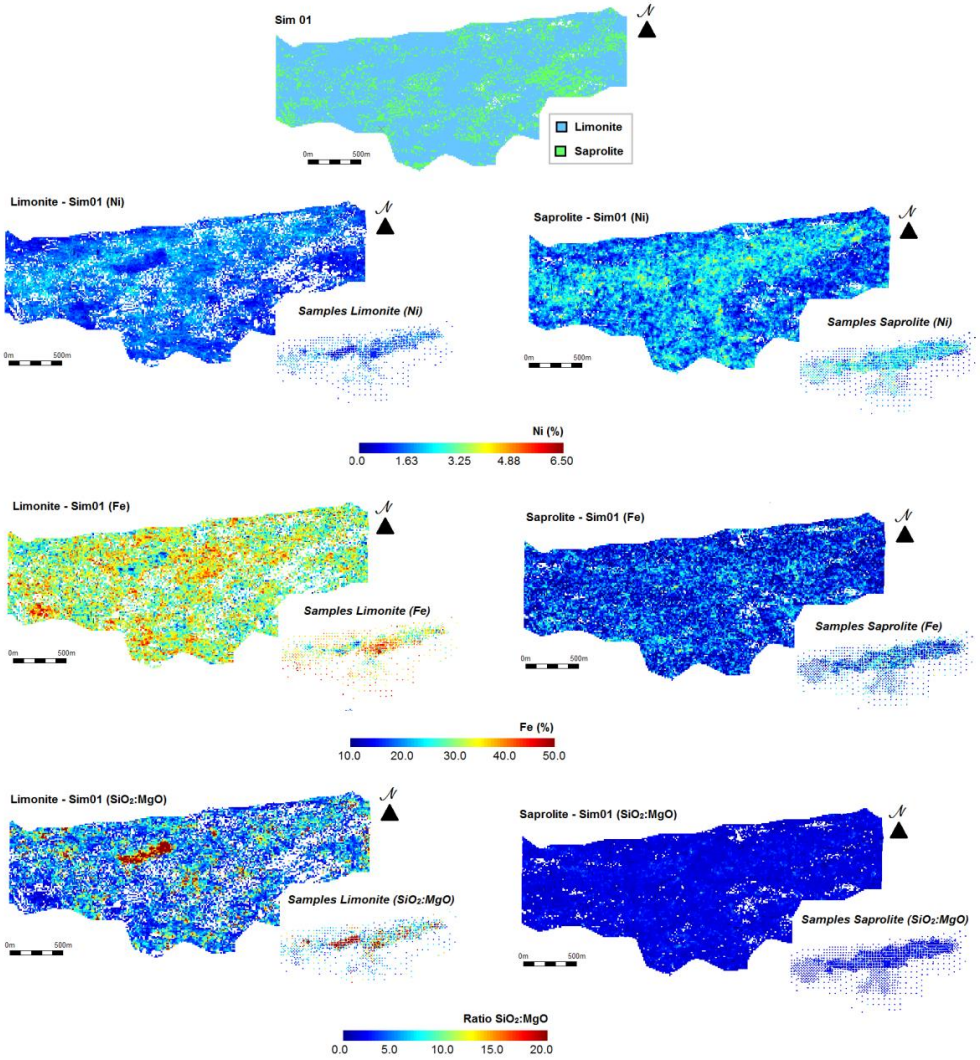

Figure 18: Different plan views for one joint simulation at block support ($12 \times 12 \times 3$ m^3). The cattegorical simulation is shown on top followed by the continuous simulations constrained by their simulated lateritic zones.

process and because of the characteristics of this pyrometallurgical process, only saprolitic ore is processed (Vale S.A., 2014). The performance of the metallurgical plant is strongly influenced by the SiO_2:MgO ratio, which for this kind of operation ought to be usually kept between 1.5 and 2.0 depending on the operational conditions, and with iron grades between 12–16% (Xavier and Ciminelli, 2008; Goodfellow and Dimitrakopoulos, 2013). The high investment associated to the mineral asset and its metallurgical complexity highlights the importance of asessing the risks by means of the jointly simulated geological scenarios in order to ensure the viability of the project.

Although the mine does not process limonitic ore, it ought to be treated as opportunity material since it contains an important amount of nickel. Therefore, to do a better assessment of the uncertainty within the *in-situ* resources, this study considers both saprolitic and limonitic ore types.

Figure 19 highlights the relative importance of saprolitic ore in terms of its nickel content. Furthermore, the graph indicates that as the Ni cut-off grade increases, the uncertainty about the tonnage of material above the given cut-off decreases. In contrast, the uncertainty about the average grades of Ni and Fe such as the Si:Mg ratio increases for both saprolitic and limonitic ore types (see Figure 20). It is noteworthy that in the approach presented here, the uncertainty regarding the tonnages incorporates both the lithological and Dry-Tonnange factor uncertainty modelled by the different geological realizations.

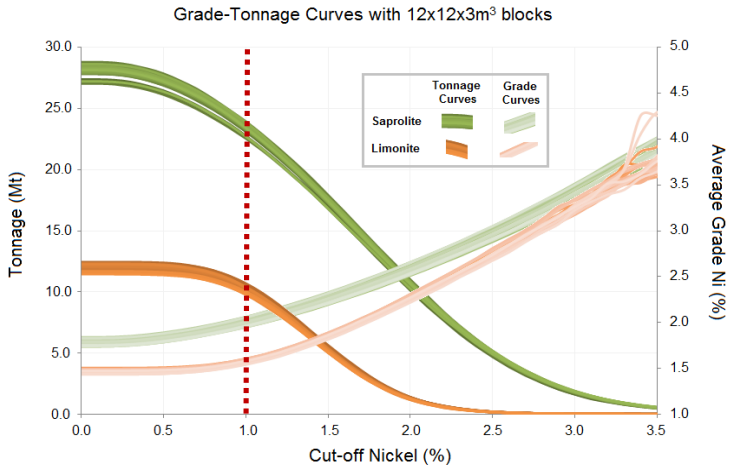

Figure 19: Grade-tonnage curves for simulated block models ($12 \times 12 \times 3$ m^3).Tonnages and Ni average grades above given cut-off grades.

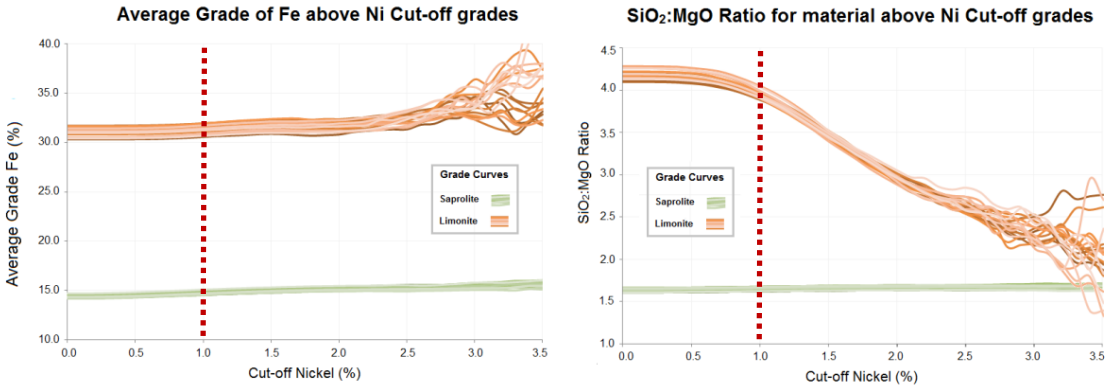

Figure 20: Fe(%) average grades (left) and SiO_2:MgO ratio (right) curves for simulated models as function of different Ni cut-off grades.

The graphs in Figures 19 and 20 show that the assessment of the global uncertainty of the *in-situ* resources can be scrutinized by integrating all the main elements to keep high performance of the metallurgical plant. For instance, if one considers an operational Nickel cut-off grade of 1.0% Ni, Figure 19 suggests that the tonnage of material above such thershold is likely to fall between 23-24Mt and 9.8-10.8Mt respectively for saprolitic and limonitic ore types, with nickel grades varying from 1.95-2.05% and 1.54-1.60% and so on. Figure 20 shows that independently of the nickel cut-off grade saprolitic ore is very likely to have iron grade and Si:Mg ratio within the range required for a ferronickel plant. However, such observations are rather limited to an assessment of global uncertainty about the *in situ* resources since grade-tonnage curves do not bring any information about local uncertainty. Therefore, they do not allow the modelling of the uncertainty of the material to be fed in the metallurgical plant during the mining operation, since it depends on the spatial variability of the deposit. Such assessment is only possible by explicitly applying the transfer-function on the stochastic simulations for the probabilistic assessment of its response parameters (e.g., stochastic mine production scheduling for assesing the uncertainty on Fe% and Si:Mg over the Life-Of-Mine as in Goodfellow and Dimitrakopoulos, 2013).

4 Conclusions

This paper showed the practical aspects of an efficient framework for joint simulation of multiple correlated variables, based on minimum/maximum autocorrelation factors in order to assess both the volumetric and multi-element uncertainty at a major nickel laterite deposit in northern Brazil.

The joint simulation of the limonitic and saprolitic weathered profiles is done by first extracting the influence of the topography though an unwrinkle process and modelling their true thicknesses. The joint simulation in two dimension is done with MAF, transforming spatially correlated geological attributes into uncorrelated service variables that can be independently simulated while avoiding the inference of a corregionalization model for the original variables. The different geological scenarios simulated for limonite and saprolite are used to constrain the joint simulation of nickel and five other correlated elements. For this purpose, the three dimensional joint simulation is carried out by applying MAF directly at block support scale. The application of such an approach required fitting only 12 variograms for the uncorrelated factors (6 for each geological unit), instead of two sets of 21 variograms and cross-variograms needed for a full model of corregionalization inside each unit. It is clear that direct simulation at block support scale is computationally more efficient and simplifies memory management during simulation of large datasets.

The output of this study is a set of multiple equally probable scenarios of the nickel laterite deposit, validated by the statistics infered from the drillhole samples. These realizations can be further used for assessment of uncertainty of *in-situ* resources, such as revealed by the graphs of grade-tonnage. Results indicate that, in overall, uncertainty about nickel and iron grades, as well Si:Mg ratio, for the *in-situ* resources is quite low. However, such observations do not guarantee the uncertainty regarding the ore feed to the metallurgical plant, that depends on local uncertainty rather than global.

Appendix A – Validation Limonite Thickness

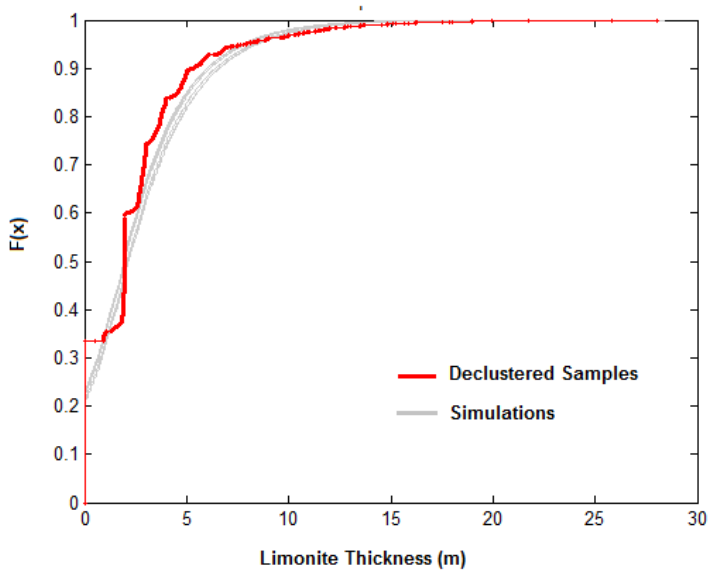

Figure 21: Cumulative distributions of declustered samples in red and simulated models in gray for the limonite thickness.

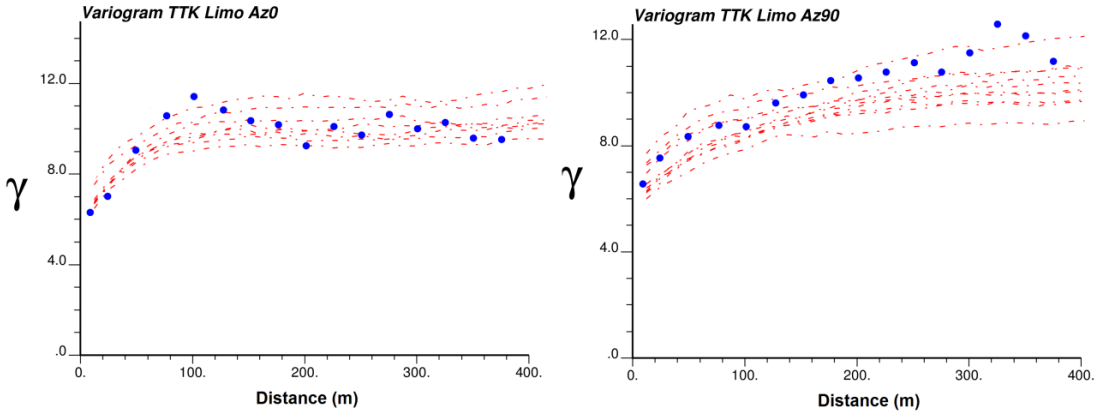

Figure 22: Experimental variogram (blue dots) and simulated models (red dashed lines) for Limonite thickness along the main directions NS and EW.

Appendix B – Variograms of MAF factors

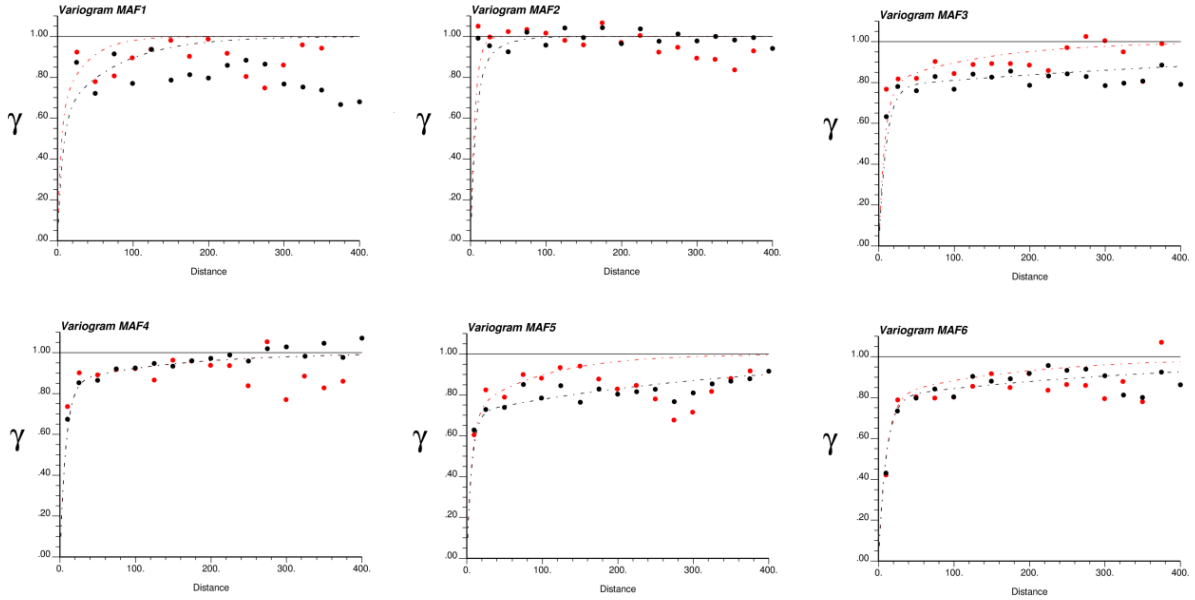

Figure 23: Saprolite – Experimental variograms (dotted) and fitted models (dashed lines) for each MAF factor along the main directions, NS (red) and EW (black).

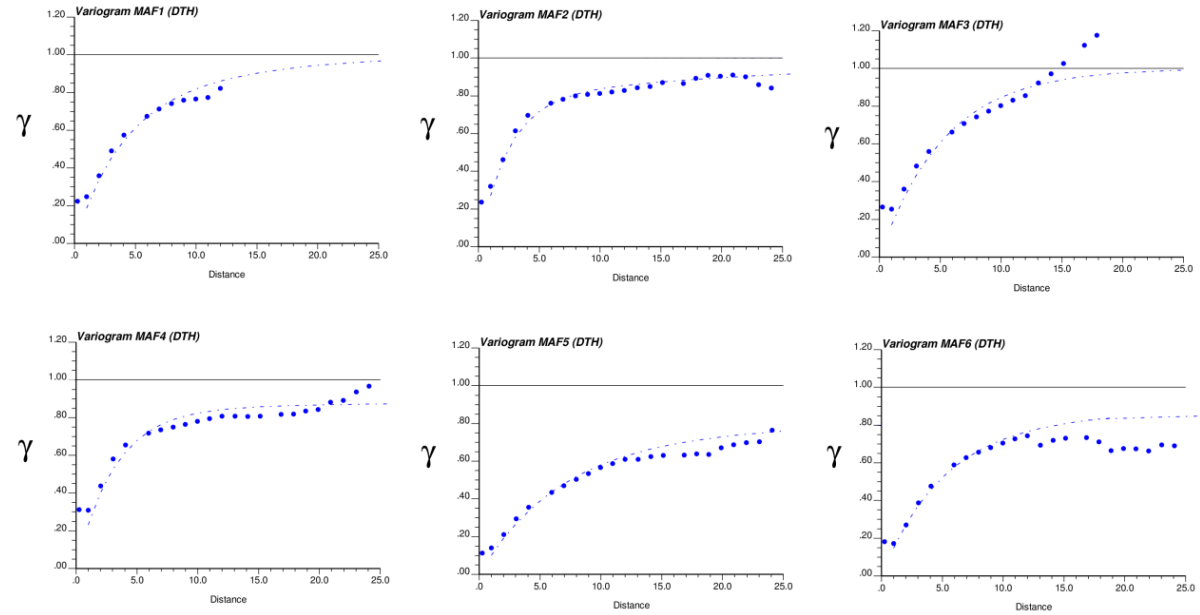

Figure 24: Saprolite – Experimental variograms (dotted) and fitted models (dashed lines) for each MAF factor along the vertical direction (DTH: “Down the Hole”).

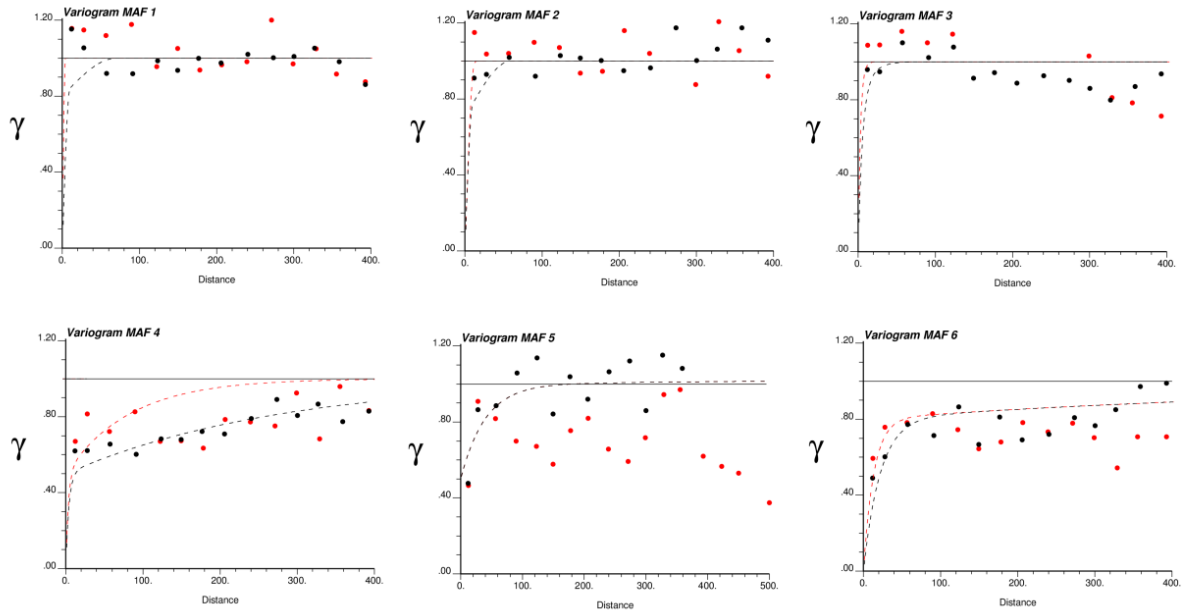

Figure 25: Limonite – Experimental variograms (dotted) and fitted models (dashed lines) for each MAF factor along the main directions, NS (red) and EW (black).

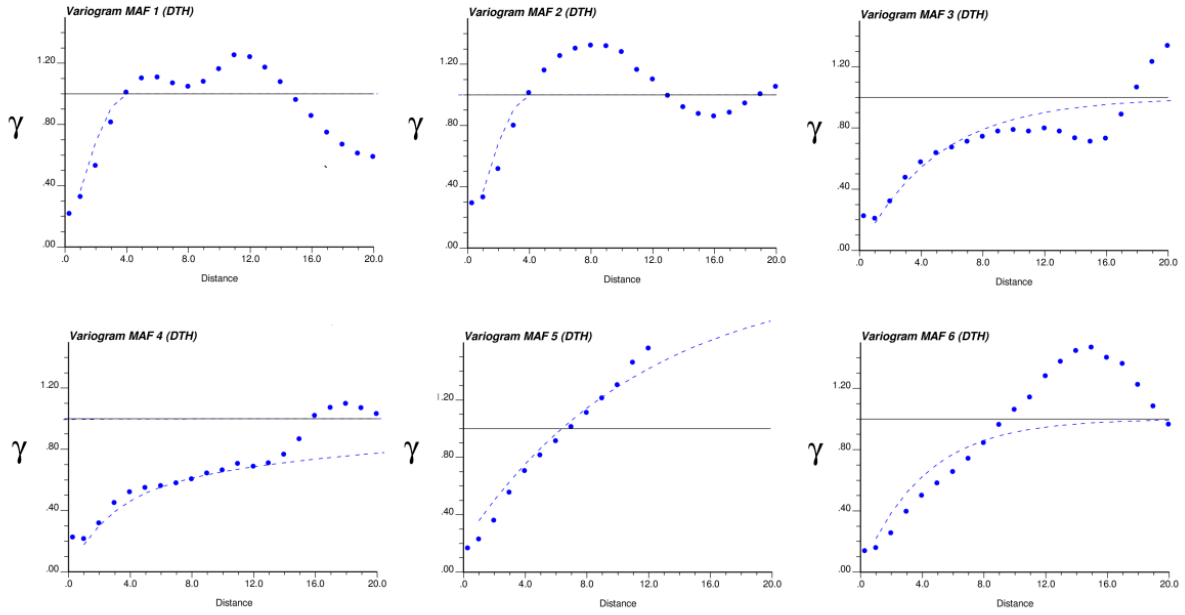

Figure 26: Limonite – Experimental variograms (dotted) and fitted models (dashed lines) for each MAF factor along the vertical direction (DTH: "Down the Hole").

References

Bandarian, E.M., Bloom, L.M. and Mueller, U.A. 2008. Direct minimum/maximum autocorrelation factors within the framework of a two structure linear model of coregionalisation, Computers & Geosciences, 34(3), 190–200.

Boucher, A. and Dimitrakopoulos, R. 2009 Block simulation of multiple correlated variables, Mathematical Geosciences, 41(2), 215–237.

Boucher, A. and Dimitrakopoulos, R. 2012. Multivariate block-support simulation of the Yandi iron ore deposit, Western Australia, Mathematical Geosciences, 44(4), 449–468.

Canico Resource Corporation 2005. Technical report: Feasibility Study Resource Estimates for Onca Puma nickel laterite deposit. [online]. Available at: http://www.sedar.com.

David, M. 1988. Handbook of applied advanced geostatistical ore reserve estimation, 216, Amsterdam, Elsevier.

Desbarats, A.J. and Dimitrakopoulos, R. 2000. Geostatistical simulation of regionalized pore-size distributions using min/max autocorrelation factors, Mathematical Geology, 32(8), 919–942.

Deustch, C.V. 2005. Practical unfolding for geostatistical modeling of vein type and complex tabular mineral deposits, in Proceedings of the 32nd international APCOM symposium, 197–202, London Taylor and Francis Group.

Dimitrakopoulos, R. and Foneca, M. 2003. Assessing risk in grade-tonnage curves in a complex copper deposit, northern Brazil, based on an efficient joint simulation of multiple correlated grades, in Proceedings of the Application of Computers and Operations Research in the Minerals Industries, 373–382, CapeTown, South Africa, SAIMM.

Dimitrakopoulos, R. and Luo, X. 2004. Generalized sequential Gaussian simulation on group size n and screen-effect approximations for large field simulations, Mathematical Geology, 36(5), 567–591.

Eggins, R.G. 2006. Modelling thickness in a stratiform deposit using joint simulation techniques, Master of Philosophy, University of Queensland, Brisbane, Australia, 1–179.

Godoy, M. 2002. The effective management of geological risk in long-term production scheduling of open pit mines, PhD thesis, University of Queensland, Brisbane, Australia, 354 p.

Goodfellow, R., Albor Consuegra, F., Dimitrakopoulos, R. and Lloyd, T. 2012. Quantifying multi-element and volumetric uncertainty, Coleman McCreedy deposit, Ontario, Canada, Computers & Geosciences, 42, 71–78.

Goodfellow, R. and Dimitrakopoulos, R. 2013. Mining Supply Chain Optimization under Geological Uncertainty. Les Cahiers du GERAD G–2013–54, HEC Montréal. Available at: https://www.gerad.ca/fr/papers/G-2013-54.

Goovaerts, P. 1993. Spatial orthogonality of the principal components computed from coregionalized variables, Mathematical Geology, 25(3), 281–302.

Goovaerts, P. 1997. Geostatistics for natural resources evaluation. New York, USA, Oxford University Press.

Journel, A.G. 2007. Roadblockstotheevaluationofore reserves – the simulation overpass and putting more geology into numerical models of deposits, in Orebody Modelling and Strategic Mine Planning - Uncertainty and Risk Management International Symposium, (ed. R. Dimitrakopoulos), 29–32, Burwood, AusIMM.

Leuangthong, O., Lyall, G. and Deutsch, C.V. 2002. Multivariate geostatistical simulation of a nickel laterite deposit, in 30th International Symposium on the Application of Computers and Operations Research in the Mineral Industry, 261–273.

Lopes, J.A., Rosas, C.F., Fernandes, J.B. and Vanzela, G.A. 2011. Risk quantification in grade-tonnage curves and resource categorization in a lateritic nickel deposit using geologically constrained joint conditional simulation, Journal of Mining Science, 47(2), 166–176.

Mueller, U.A. and Ferreira, J. 2012. The U-WEDGE transformation method for multivariate geostatistical simulation, Mathematical Geosciences, 44(4), 427–448.

Myers, D.E. 1989. Vector conditional simulation, in Geosatistics (ed. M. Armstrong), 283–292, Avignon, France, Kluwer Academic Publishers.

Peattie, R. and Dimitrakopoulos, R. 2013. Forecasting Recoverable Ore Reserves and Their Uncertainty at Morila Gold Deposit, Mali: An Efficient Simulation Approach and Future Grade Control Drilling, Mathematical Geosciences, 45(8), 1005–1020.

Rondon, O. 2012. Teaching aid: minimum/maximum autocorrelation factors for joint simulation of attributes, Mathematical Geosciences, 44(4), 469–504.

Switzer, P., Green, A.A., 1984, Min/Max autocorrelation factors for multivariate spatial imaging, Technical Report No. 6, Department of Statistics, Stanford University, 1–14.

Tercan, A.E. and Sohrabian, B. 2013. Multivariate geostatistical simulation of coal quality data by independent components, International Journal of Coal Geology, 112, 53–66.

Vale S.A., 2014. Annual report 2013. Available at http://www.vale.com/EN/investors/information-market/annual-reports/20f/20FDocs/20F_2013_i.pdf.

Wackernagel, H. 2003. Multivariate Geostatistics: An Introduction with Applications (3rd Ed.), Berlin, Springer.

Xavier, F.M.R.S. and Ciminelli, V.S.T. 2008. Development of technical and economic parameters affecting process selection to treat nickel laterite ores, in Hydrometallurgy 2008: Proceedings of the Sixth International Symposium (eds. C. Young, P. Tay and C. Anderson), 532–540, Littleton, Society for Mining, Metallurgy, and Exploration.